HIGH VISCOSITY JETTING OF CONDUCTIVE AND DIELECTRIC PASTES FOR PRINTED ELECTRONICS

J. Ledesma-Fernandez, C. Tuck, R. Hague

Additive Manufacturing and 3D Printing Group, University of Nottingham, NG7 2RD, UK
REVIEWED

Abstract

Ink-jet printing of multiple materials in 3 dimensions is a promising alternative to traditional patterning methods due to its flexibility, scalability and accuracy. However, the printability of the inks is strongly restricted by material properties such as surface tension and viscosity. Dispensing high viscosity fluids on a drop-on-demand approach is a potential solution that can facilitate the incorporation of new materials to the jetting catalogue. Consequently, in this study 2 micro-dispensing valves are used in combination with a mechanical stage to deposit conductive and dielectric pastes with viscosities of 15.3 ± 0.2 and 0.638 ± 0.005 Pa·s (at 25°C and $10 \ s^{-1}$ shear rate) respectively. Crucial printing parameters such as pressure, temperature, pulse shape and drop spacing are studied in order to optimise the process. Additionally, post-printing characteristics such as contact angle of different materials and cured layer profiles are also measured and taken into account during the designing of the 3D patterns to minimise the negative effects of the thickness miss-match of different materials. Finally, the manufacturing capability of the set-up is demonstrated by the fabrication of a functional device using a combination of "pick-and-place" components and high viscosity jetting.

Introduction

Additive Manufacturing offers numerous advantages over traditional fabrication such as customizable parts, increased design freedom or complex parts at no extra cost. These are only a few of the characteristics that have contributed to the great expansion of Additive Manufacturing during the last decade. However, most systems are only capable of fabricating objects with a single material at a time, which limits the functionality of the final part. Therefore, to fully take advantage of the capabilities of Additive Manufacturing the incorporation of multiple materials in a single process is required. This approach has already been explored for some additive technologies such as multi-nozzle FDM [1], inkjet-infiltrated porous parts built by Laser Sintering [2] and stereolithography performed with exchangeable resin vats [3]. However, although these approaches are a step forward in their respective fields, there are situations where other Additive Manufacturing techniques may be required.

An alternative technology capable of multi-material fabrication is inkjet printing, which fundamental principle of depositing small drops of fluids in precise locations on demand is ideal for the creation of complex patterns with local variations of material concentration. This capability of creating "digital materials" by combining a finite number of primary inks was first commercialised by Objet Geometries Ltd. in early 2000 [4]. However, the capabilities of inkjet are not limited to the deposition of polymers and many other materials have been jetted in the last decades. Particularly, in the field of conductive materials inkjet printing has also been used to create functional transistors [5], strain sensors on fabric [6] or low-cost Radio-frequency

Identification (RFID) tags [7] among many other examples. This has led to the rise of printed electronics, which is a potential solution for low-cost and customized products.

However, inkjet printing imposes great restrictions to the properties of the inks that need to be finely formulated to avoid nozzle clogging, present long stability and behave according to predictive models during the printing process. One consequence of these boundaries is that the viscosity of the inks needs to remain typically under 25 mPa s, which limits the molecular weight of the used polymers and the solid content of particulate inks. This not only narrows considerably the material catalogue but also forces the addition of rheological modifiers such as solvents and surfactants [8] that alter the properties of the deposited tracks. This is especially relevant in the case of conductive materials, where the organic elements added to improve the processability of the ink need to be removed during a post-processing step to allow the percolation and/or sintering of the conductive particles dispersed on the ink.

A high viscosity non-contact approach would allow the printing of materials with higher solid content, which can translate into reduced volumetric shrinkage, increased mechanical properties and improved conductivity. This has been explored with different approaches such as aerosol jet [9], where the material is atomized in a pressurized chamber previous deposition; acoustic inkjet, where an ultrasonic perturbation is focused on the fluid free surface to induce the creation of droplets without the need of a nozzle [10]; and ultrasonic droplet generation, where the nozzle plate is specifically designed to focus the acoustic waves generated by a piezoelectric actuator and produce the ejection of droplets [11]. Additionally, jetting valves that combine pneumatic pressure and mechanical actuation have also been used to create 2-dimensional patterns in a continuous inkjet approach [12]. In this work a similar jetting valve is used to deposit two fluids of high viscosity in a drop-on-demand approach to create 2D and 3D geometries. The different stages of drop formation, deposition and post-treatment of 2 materials are studied and their application for multi-material jetting is demonstrated by the creation of a proof-of-concept sample including embedded conductive tracks and an LED.

Materials and Methods

High viscosity printing system

The set-up consists of a computer controlled 3-dimensional stage with an overall accuracy of 5μm that controls the ejection and position of 2 PICO xMOD micro-dispensing valves (Nordson EFD). The system is equipped with a digital camera to monitor the printing stage and select the printing origin. A UV-lamp (FireFly 25x10, Phoseon Technology) was installed to enable photo-curing of materials during the process. The software is based on a combination of C# and XML and is in charge of printing parameters such as printing speed, drop spacing and curing speed. This code also communicates with the digital controller (Nordson EFD) that provides the printing signal to the valves.

The working principle of the jetting valves is based on the combination of pneumatic and mechanical actuation. Precisely, the fluid is pressurized (up to 0.6 MPa) and injected on the jetting chamber along a fluid path that can be heated up to 100° C. There, a piezoelectrically driven piston ended with a ceramic sealing ball is oscillated according to the printing signal (up to 500 Hz), opening and closing the nozzle as a consequence. These driving pulses are mainly

described by its pulse time (t_p) and cycle time (t_c), which are both under user control through manipulation of the digital controller, and the opening and closing speed of the valve, which is not under user control but can be selected from a limited amount of pre-sets. This mechanism allows the ejection of materials in the range of 50 – 200.000 mPa s [13]. A schematic illustration of this system is shown in Figure 1 together with a description of the structure of a train of printing pulses.
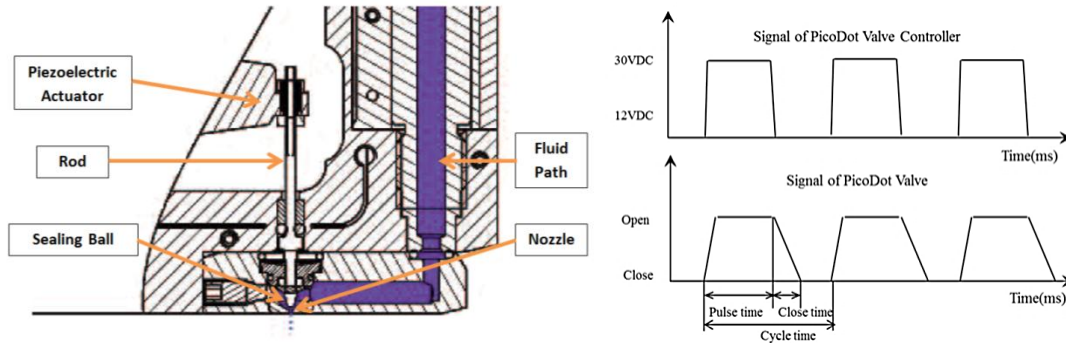
Figure 1: (Left) Schematic illustration of the PICO valve with a description of its most relevant parts. Modified from valve user manual [13]. (Right) Typical shape of the driving pulse showing the effect of the pulse, close and cycling times on the state of the valve [12].

High viscosity printing system

The **viscosity** of the materials was measured with a Kinexus Pro rheometer (Malvern Instruments Ltd.) with a cone-plate configuration. A shear rate of $1 - 50$ s^{-1} was used for the carbon paste while a range of shear rates of 1-100 s^{-1} was applied to the photo-reactive resin. The range of temperatures was $25 - 40$ °C, which is within reach of the micro-dispensing valve.

The **surface tension** of the fluids was characterised with a Drop Shape Analyser (DSA100, Krüss) and a G18 stainless steel blunt needle, using the Pendant Drop Method and the Laplace-Young model provided by the built-in software (Drop Shape Analysis, DSA4). Ten droplets of each fluid were measured at 21.5 ± 0.1 °C to obtain an average value $\pm$ standard error of the surface tension.

The **density** of the fluid was calculated by depositing known volumes of material with a syringe of 0.1 ml precision and measuring the variation in weight using an analytical laboratory balance (SI-234 Denver Instrument) at an ambient temperature of 19.8 ± 0.1°C. A linear regression was later performed to obtain the density value $\pm$ standard error.

Jettability and deposition study

The drop footprints resulting from different parameter sets were studied with an optical microscope (Eclipse LV100 ND, Nikon) to study the jetting behaviour of **high viscosity** fluids. Later, the jetting process related to selected parameter configurations were recorded with a high speed camera FASTCAM APX RS (Photron Inc.) illuminated by a collimated light source (OSL2 Fiber Illuminator, Thorlabs).

Post-process investigation and performance test

UV-curable materials were post-processed with a **UV-lamp** of 2 W/cm^2 peak irradiance and 380 – 420 nm output (FireFly 25x10, Phoseon Technology) at 4.0 mm ± 0.1 mm of the printing platform. Materials requiring evaporation of solvent between layers where left to dry under controlled circumstances.

The study of the **profile of multi-layered samples** was performed with a surface profilometer (Surftest SV-3100, Mitutoyo), taking linear profiles at different points in the sample. Moreover, the profile of UV-curable multi-layered structures was also observed with an optical microscope (Eclipse LV100 ND, Nikon) and a sample holder that allowed the observation of the edge of the printed samples. Their height was measured with an electronic outside micrometer (Schut Geometrical Technology) of 0.001 mm of precision 3 times to obtain the average value ± standard error.

To calculate the **resistivity** of conductive materials several tracks were printed with different number of layers and left to dry at room temperature and pressure for 24 hours. Their resistance was measured 6 times using a digital multimeter (TENMA), accepting the average ± standard error as the resistance of that particular track. Then, their cross section was measured with a contact profilometer as previously explained. Finally, the resistivity value was obtained from a linear fit of these results, taking into account the definition of resistance [14]:

$$R = (l \cdot \rho) \cdot \frac{1}{A} \tag{1}$$

Where R is the resistance of the track, l its length, ρ is the resistivity of the material and A the cross-section of the sample.

Multi-material interaction and proofs-of-concept

The **contact angle** of a material on different substrates was measured with a Drop Shape Analyser (DSA100, Krüss) equipped with a G18 stainless steel blunt needle, using the Sessile Drop mode and the fitting method of the "tangent". Each measurement was taken after a minute of the drop ejection, which is a realistic time scale of the printing process. The **substrates** consisted on an untreated glass slide, a clean piece of Polycarbonate film (Makrofol, Bayer) and a glass slide coated with 40 µm of one of the printing materials using a K Hand Coater (RK PrintCoat Instruments Ltd.) and applying the corresponding post-treatment of each material.

Materials

The **conductive material** used for the set of experiments presented in this work is a commercial carbon paste (Electric Paint, Bare Conductive). A transparent photo-reactive resin (Clear, Formlabs) originally intended for stereolithography was selected as a structural material. The **embedded LED** used in the embedded electronics proof-of-concept was a green PICOLED (P12 Series, ROHM) of 1.0 x 0.6 x 0.2 mm and was place manually with a pair of tweezers between printing cycles. Its position was checked with the mounted camera of the printing stage and it was powered using 3 standard AA batteries.

Results and discussion

Material characterization

The **viscosity** of the carbon paste was studied at different shear rates and temperatures, as can be seen in Figure 2. An increase on the shear rate is observed to cause a noticeable decrease of the viscosity, which is known as "shear thinning" and is common in polymeric composites with solid filling [15]. The viscosity is also reduced when the material is heated, however this needs to be taken carefully since temperatures greater than 35°C have been observed to cause quick evaporation of the solvent on the nozzle, leading to blockages. Therefore this material was printed at 25°C. Similarly, the viscosity of the photo-reactive resin was studied (Figure 3) and the same trend of reduction in viscosity with increased temperature was observed. Nevertheless, the rheological behaviour of this material at increased shear rates is different than the conductive material, since the viscosity is maintained constant after a small initial reduction at shear rates below $3s^{-1}$. This behaviour is typical from Newtonian fluids but a measurement of the viscosity at a broader shear rate range is required in order to confirm this observation.
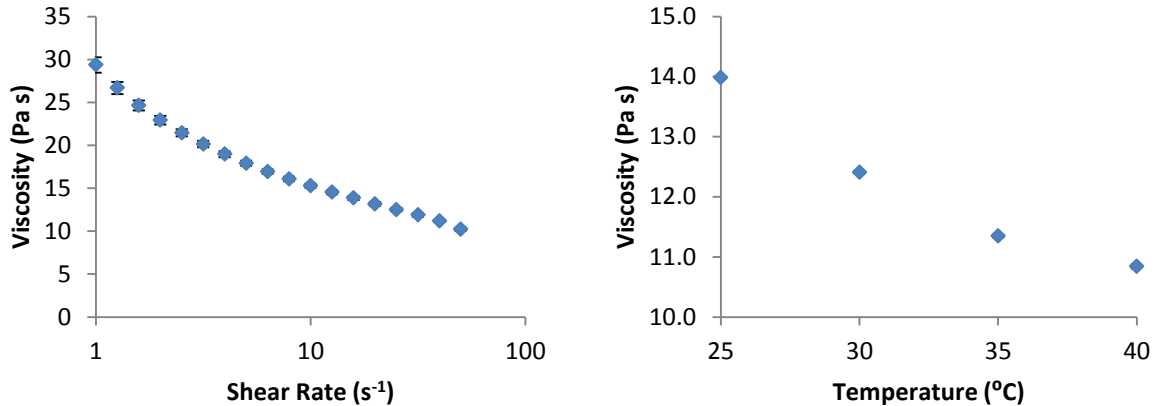
Figure 2: Viscosity of a carbon paste measured with a rheometer in a cone-plane configuration. (Left) Constant temperature (25°C) and shear rates between 1 and 50 s^{-1}. (Right) Constant shear rate (10 s^{-1}) but different temperatures in the range of 25 to 40°C.
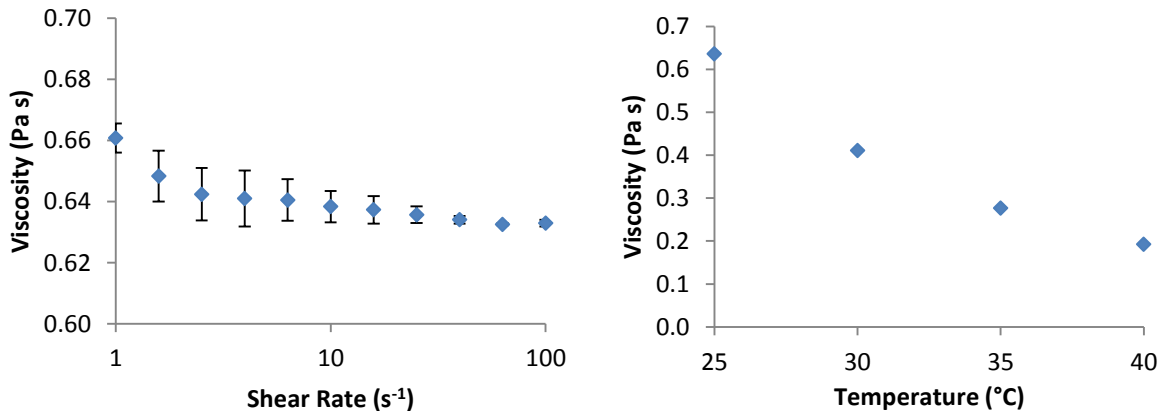
Figure 3: Viscosity of a photoactive resin measured with a rheometer in a cone-plane configuration. (Left) Constant temperature (25°C) and shear rates between 1 and 100 s^{-1}. (Right) Constant shear rate but different temperatures in the range of 25 to 40°C.

Additionally, the **surface tension** and **density** of these materials were characterised (Table 1). These materials show viscosities above the threshold of 25 mPa s typically accepted for piezo based inkjet techniques and could not be jetted in a commercial inkjet printer.

Table 1: Summary of relevant material properties of the fluids used in this work

	Carbon Paste	Photo-reactive Resin
Viscosity @ 10 s^{-1},25°C (Pa s)	15.3 ± 0.2	0.638 ± 0.005
Surface Tension (mN/m)	57.8 ± 1.8	34.9 ± 0.2
Density (g/ml)	1.254 ± 0.016	1.038 ± 0.012

Jettability and Deposition study

In this work, the distance between the nozzle and the substrate at any given time is referred as **gap size.** Figure 4 shows droplets of carbon paste jetted at different heights from the substrate. It can be observed that gap sizes larger than 1 mm result in the splash of the droplet on impact, which negatively affects the printing resolution. Therefore, the gap size was kept at 0.8 mm for the rest of this work. Likewise, the behaviour of photo-reactive resin were studied at different gap size but no clear difference in the drop size or shape was observed in the rage of 0.5 to 3 mm, therefore the 0.8 mm gap was also used for this material.
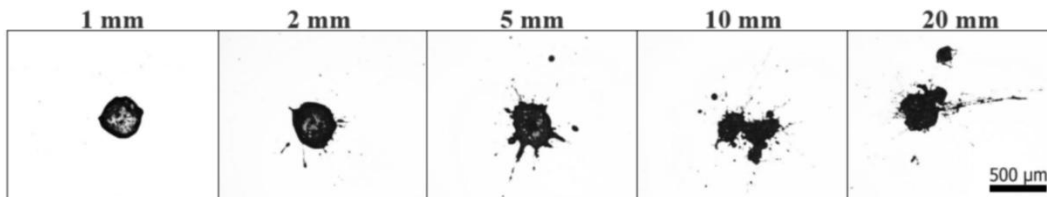
Figure 4: Individual drops of carbon paste impacting on a polycarbonate substrate at different distances from the nozzle imaged by reflexion microscospy.

In a similar way than the gap size, different **pressures and valve closing times** were tested by printing arrays of 6 x 6 unconnected drops and studying their size and shape with a reflection microscope (Figure 5). From these sets of images it can be concluded that the size and shape of the drops is not visibly affected by the **pressure** in the range of 0.1 to 0.5 MPa. A further investigation conducted with high speed videos of the printing process showed that the ejection only happens at the end of the pulse time, i.e. during the closing time of the valve. This means that the applied pressure is not enough to push the material through the nozzle even when it is open and its main role is to fill the nozzle chamber to prevent material stagnation, as it was previously observed by Yang et al. 2013 during their study of the ejection of fluids of different viscosities with a valve similar to the one used in this work. Alternatively, Figure 5 also shows that the **closing time** is clearly the driving factor in this viscosity range, which is also in agreement with the explanation of Yang et al. 2013. It is observed that for the carbon paste the profile with a closing time of 400 µs does not provide enough kinetic energy to produce a clean ejection; instead, as it was observed on the high speed videos, the tail of the drop breaks after the landing of the drop, collapsing over the substrate in an uncontrolled way. On the contrary, the

profile with 120 µs produces bigger drops with good repeatability but still shows signs of splashing due to its excessive closing speed. The profile with a closing time of 200 µs provides smaller drops and good repeatability across different pressures for both materials, which will lead to a higher printing resolution. Conversely, less influence of the closing time is observed for the UV-curable resin, where circular drops are obtained for the profiles with closing times of 200 µs and 120 µs. However, this good printing performance is abruptly interrupted when the closing time goes over 200 µs, which was tested several times without success. Nevertheless, this was only attempted in the range of pressures tested in this experiment and it is not ruled out that a higher pressure can force the ejection with these slow closing profiles but an investigation of the printability at higher pressures was not in the scope of this work. Consequently, the profile with 200 µs and the pressure of 0.1 MPa is selected for both materials with associated drop diameters of 591 ± 2 µm and 391 ± 2 µm for the photo-reactive resin and the carbon paste respectively.

Figure 5: Optical study of drop arrays of (left) a carbon filled polymer and (right) a photo-reactive resin with the pressure of the valve changing for each column and a different valve closing time in each row.

A general overview of the jetting and deposition stages was recorded at 18000 fps for each material with the printing parameters that have been selected along this report. In these videos is observed that the material travels from the nozzle to the substrate in one frame for the carbon paste (Figure 6) and two for the UV-curable resin (Figure 7), which can be used to provide a minimum boundary of the average speed of the drops of 14 m/s and 7 m/s respectively. This estimation can be greatly improved analysing videos at a higher frame rate, which will be performed in future work. From Figure 7 it can also be seen how the greater speed of the carbon paste helps detach the jet tail that stays connected to the nozzle during almost 3 ms in the case of the photo-active resin. This need to be taken into account when the printing speed is selected, because if the head moves when the tail is not separated from the nozzle, non-circular droplets will be obtained due to the uncontrolled collapse of that body of fluid. A good example of this can be found in Figure 5, where the slowest closing speed of the valve created this effect on the carbon paste regardless the pressure. Furthermore, Figure 7 shows that even though the presence

of the tail may cause problems with the UV-curable resin, this material recombines faster and more homogeneously than the carbon paste, which can be appreciated at the final frames of each material. Specifically, the carbon paste changes the shape of the material deposited but it is unable to form something close to a spherical cap under 3 ms, while the photo-resin would be almost done in less than 2 ms if the jetting tail were not present. This may also explain why the surface of the UV-curable material is always smoother than the carbon.
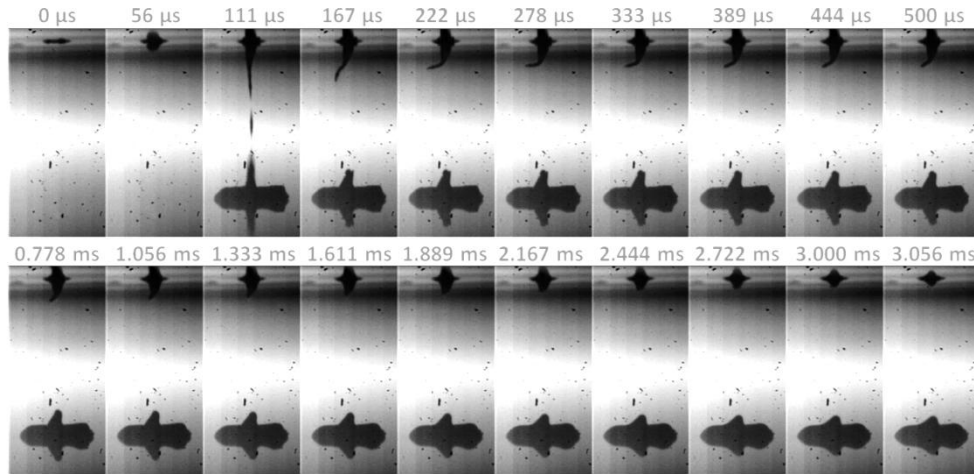
Figure 6: Printing events for the carbon paste with a gap size of 0.8 mm. Videos recorded at 18.000 fps and 4.06 µs of shutter speed.
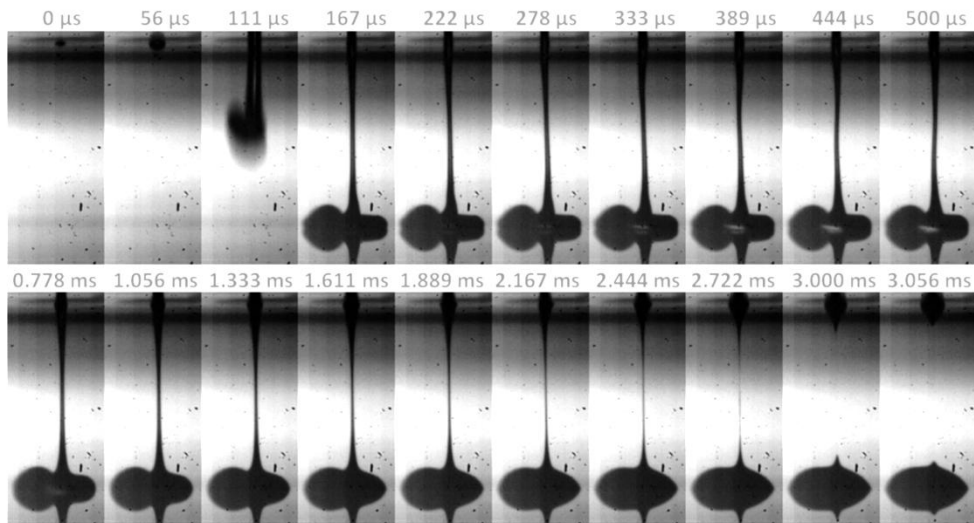
Figure 7: Printing events for the photo-reactive resin with a gap size of 0.8 mm. Videos recorded at 18.000 fps and 4.06 µs of shutter speed.

Once the ejection and deposition of individual drops was studied, several square patterns with **different values of DPI** (drops per inch) were produced in order to find the drop spacing for each material that yields features with connected drops, no internal holes and edges as sharp as possible. In the case of the carbon paste (Figure 8), unconnected drops are observed at small DPI and more defined edges are obtained as the drop space is reduced. However, instead of focusing

47

only on these 2-dimensional deformations it is important that we focus on the 3D aspect of these samples, understanding the DPI not only as a measurement of droplet spacing but also as magnitude directly related with the deposited volume on a given area. This way, it is possible to observe that the thickness and curvature of the surface of the squares are notably incremented at higher DPIs, which in the pictures can be perceived by the variation in the light reflection. This may seem a positive effect keeping in mind that the focus of this work is creating 3D structures, but these kind of curved surfaces will affect the wetting of the following layer, which in turn affect the next one and so forth, leading ultimately to domed geometries. Accordingly, the DPI for the carbon paste was chosen as 100 for the rest of the experiments.

The case of the photo-resistive resin (Figure 9) seems different because bulging of the squares surface is not apparent but a strong dependence between the DPI and the surface roughness is observed instead. It is important to remember that each material has been post-treated to induce solidification using a different approach. Particularly, the carbon paste solvent evaporation was accelerated by heating the printing platform at 35°C, while the resin was cured using a UV-lamp placed at 4mm and moving over the pattern one time at a curing speed of 150 mm/s. It is believed that precisely the curing step, even applied during a time as short as the one used in this experiment, may have caused shrinkage on the sample, causing the material on some edges to retract (as can be seen in Figure 9) and the middle to the sample to shrink in a repeatable pattern. Nevertheless, this effect can be reduced controlling the amount of fluid deposited per unit of area, as can be observed for the sample with a corresponding DPI of 60, which does not have sharp edges but does not display a strong texture on its surface either. Therefore, from this moment onward the DPI for the clear resin will be limited to 65.
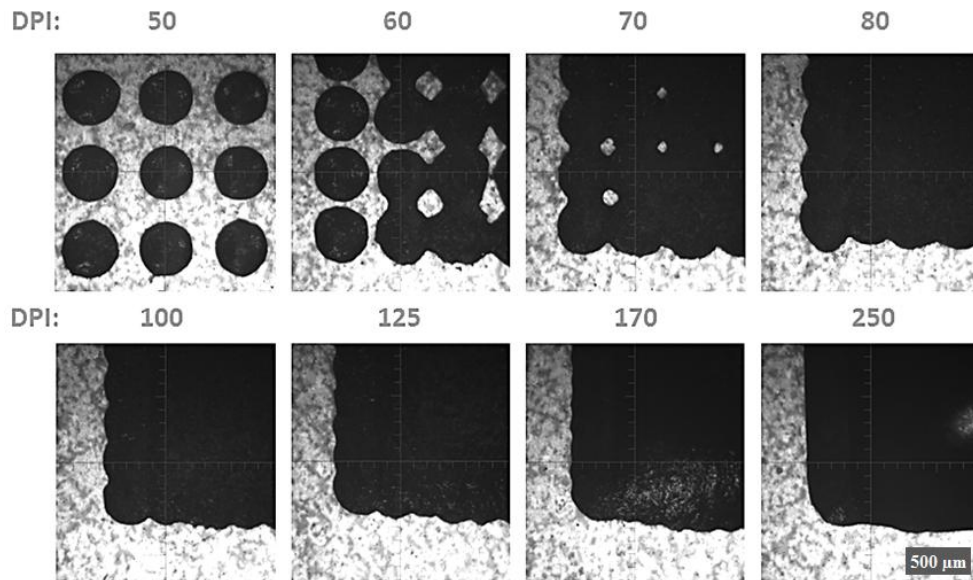

Figure 8: Printed arrays of carbon paste droplets with different DPI. An increase in the height of the sample can be appreciated due to the change in the reflection of the surface of the high DPI squares.

48
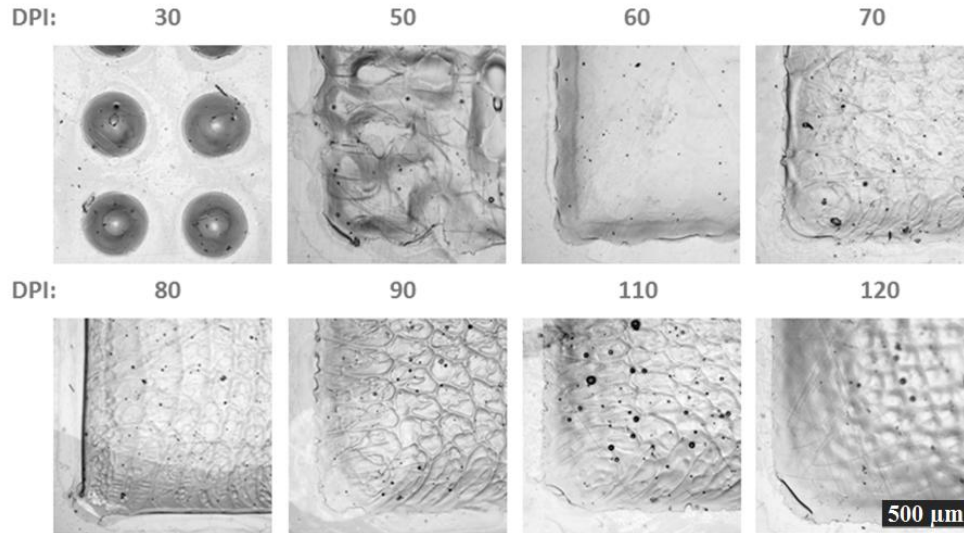
Figure 9: Printed arrays of UV-curable droplets with different DPI. The size of the scale bar is 500 μm. An increase in the texture of the surface can be appreciated at DPIs greater than 70 but sharp edges are not formed at DPI lower than 60.

Post-process investigation and multi-layer tests

In order to study the layer thickness of the carbon paste and the influence of the drying time in the printing process, 8 tracks of an increasing number of layers from 1 to 8 were printed leaving 0 s, 30 s and 300 s between layers. These drying times, however, refer to the time programmed to stop the printing process completely on the modified software and would have to be added to the time that the machine uses to clean and reposition the head between layers in order to obtain an absolute measurement of the time between the deposition of the last drop on one layer and the first drop of the next one. The results are shown in Figure 10, where it can be observed that the optimum drying time that minimises the spreading of the paste and leads to the most significant growth in the z-direction is between 31 and 300 s, since both the 0 s and 30 s samples display bulged tracks as a clear effect of excessive fluid per layer. These conclusions however cannot be generalised since the drying time is strongly related with the area exposed to air, which in turn would depend on the particular pattern. Nonetheless, this test provides a good estimation for processing purposes and will be repeated in the future for different post-treatment methods to compare with the non-accelerated evaporation here shown.
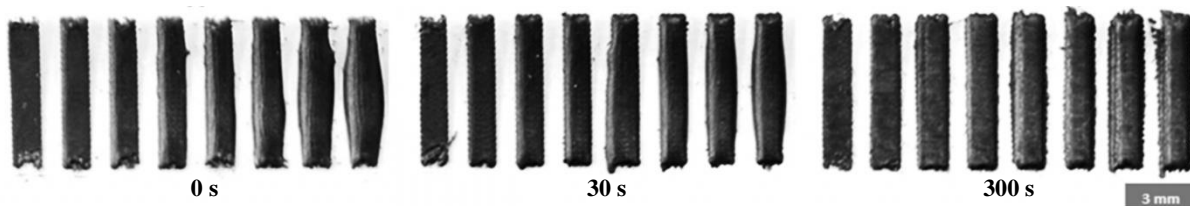
Figure 10: Carbon multi-layered samples printed with a different waiting time between layers to study the effect of the evaporation time on the geometry of the tracks. The first tracks on the left have only one layer but an additional one is added in each track up to 8 layers. Later, these samples were also used to calculate the resistivity of the material, which explains the marks that the multimeter probes left on some of the samples.

49

After 24h of drying at room temperature, the sample printed with a programmed drying time of 300s was analysed with a surface profilometer (Surftest SV-3100, Mitutoyo) to obtain the values for layer thickness shown in Figure 11. A value of 53.6 ± 0.6 μm for the thickness of each layer was obtained applying a linear fit to the height of the tracks and it will be used as the increment in the Z-axis per printed layer from now on. Additionally, comparing the measured resistance of each track with the average cross-sectional area provided by the contact profilometer, the resistivity of the carbon paste was calculated. Figure 11 also shows the mentioned plot of the resistance against the reciprocal of the area of each track, applying equation (1), from the slope of its linear fit a value of $(1.09 \pm 0.03) \cdot 10^{-2}\, \Omega\, m$ was calculated for the resistivity of the carbon paste. This result is comparable to the reported volume resistivity for carbon black conductive filament for fuse deposition modelling $(9 - 12 \cdot 10^{-2}\, \Omega\, m$)[16]. However, the measured value is still six orders of magnitude bigger than the resistivity of bulk silver $(1.587 \cdot 10^{-8}\, \Omega\, m$ at 20°C) [14]. Nonetheless, this is a limitation strictly based on the used material and not the set-up, which potentially can be used to deposit more conductive materials.
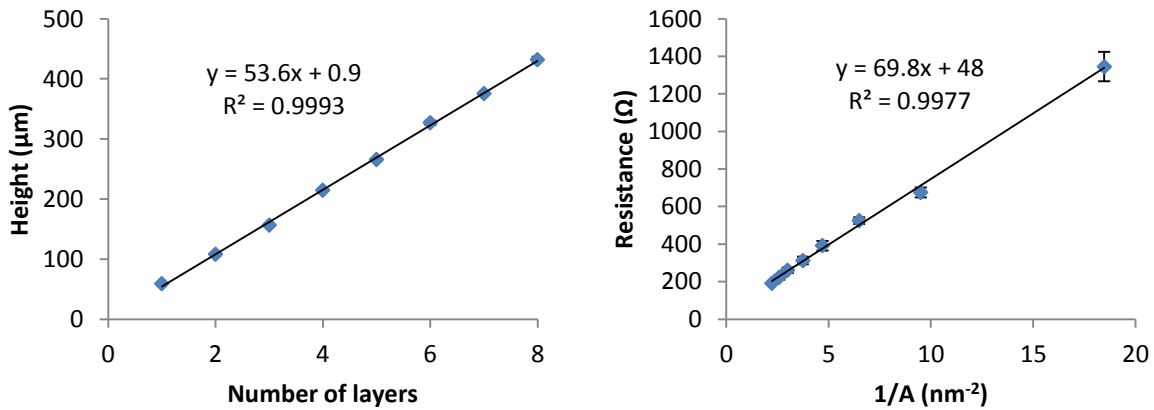
Figure 11: (Left) Linearity of the layer thickness on multi-layered carbon samples with 300 s of drying time per layer. (Right) Resistivity calculation of the carbon paste based on the comparison between their individual resistance and the cross-sectional information obtained from contact profilometry.

The profile of multi-layered samples of **photo-reactive resin** was studied by printing samples of 30 layers with different curing speeds, i.e. the speed of the UV-lamp over the printed pattern, to check the influence on the final geometry of this parameter. The profile of the structures was observed with a reflection microscope (Figure 12) and their height was measured with an electronic micrometer (Table 2). These results indicate that a curing speed of 150 mm/s at a distance of 4 mm from the sample is enough to cure the material and prevent it to flow before the deposition of the following layer, leading to analogous results than slower curing speeds. This speed could be potentially increased but it will not reduce significantly the length of the process since the longest stage is the printing, which is limited to a maximum of 500 Hz. Additionally, assuming linearity of the increase of the sample height with the number of layers it is possible to estimate the layer thickness of this material (Table 2) in order to use it in the multi-material samples printed in the last section of this work. These multi-layered samples also revealed another interesting behavior of the UV-curable resin, since in the 3 cases there are some dark lines crossing the sample perpendicular to the substrate with a fairly constant frequency. A closer study revealed that the distance between these vertical patterns is 400 ± 20 μm. This value is in

agreement with the drop spacing corresponding with a DPI of 65, which is 391 μm. Therefore, it can be assumed that this pattern is created due to the air bubbles produced and trapped due to the impact of the resin during the drop deposition stage. However, if we look back to Figure 9, this pattern is not appreciated in the single layer there studied, which leads us to believe that the roughness of the previous layer is in fact the driving factor of this effect.
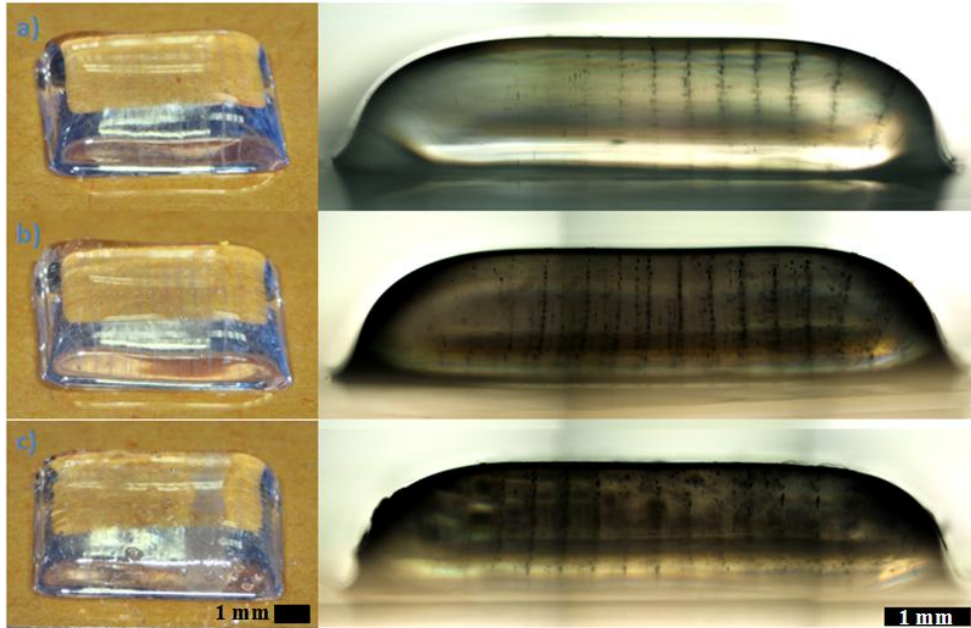
Figure 12: Cuboids of photoactive resin with 30 layers. Each structure was cured at a different speed, therefore limiting the radiation dose of the sample. The used curing speeds were a) 150 mm/s, b) 30 mm/s and c) 6 mm/s. The profile was investigated via optical imaging.

Table 2: Height and estimated layer thickness corresponding to structures of photo-resin with 30 layers UV-cured at different speeds.
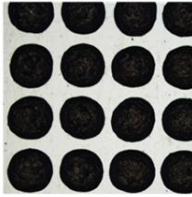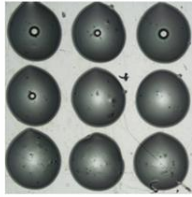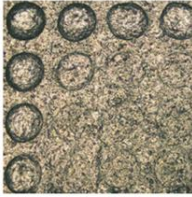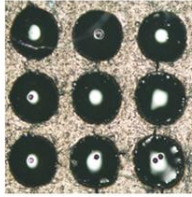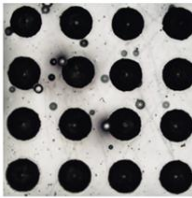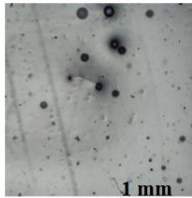
Curing Speed (± 1 mm/s)	Height (± 0.007 mm)	Layer thickness (± 0.2 μm)
150	1.415	47.2
30	1.403	46.8
6	1.398	46.6

Multi-material tests and proof-of-concept

The previous tests were performed for each material individually but in a real multi-material printing situation this would not describe the process accurately. Therefore, tests involving various materials need to be carried out to assess their combined behaviour. In the present work the focus is placed on the different wettability of each material on different substrates, which can lead to variations to the layer thickness than what was previously observed. Consequently, the contact angle of droplets deposited on different substrates was tested and presented in Figure 13. Here it can be observed that the UV-curable resin wets more than the carbon paste in all situations, explaining its bigger footprints. Moreover, there is a clear

difference between the case of carbon on a carbon substrate and the UV-curable material deposited on itself, which clarifies why the structures printed with carbon presented sharper edges than the ones created with the resin. However, the conclusions extracted from this study can only describe trends and should not be extrapolated to the printing situation straight away. This is mainly due to the difference on the roughness of hand coated and printed substrates but also due to the great difference between the volume of the droplets used in this study (in the range of microliters) and the ones involved in printing (nanoliters).

Figure 13: Spreading behaviour of the 3 materials used in this work in different combinations. (Left) Contact angle of deposited drops using a Drop Analysing System. (Right) Top image of samples printed with the micro-dispensing valves used in this work. The substrates were also printed and post-treated accordingly.

Following this reasoning, another matrix of material combinations was created using the printing set-up to assess the variation of the drop diameter instead of its contact angle, as can also be found in Figure 13. This experiment confirmed that the carbon paste wets all the surfaces less than the photo-reactive resin, leading to smaller drops. The sample of carbon paste on a carbon substrate displayed individual drops on the edge of the sample but none in its middle, which seems to be an indication that the substrate material may not have been totally dry on the centre and facilitate the spreading of the drops. Nevertheless, the drops that were left are smaller than the ones printed directly on the polycarbonate film, as it was anticipated by the contact angle in these materials (Figure 13). Additionally, a contradiction of the previous observations regarding the spreading of the carbon paste on a photo-resin substrate was found, since the drops of carbon are the smallest on this substrate. This may be related, as previously discussed, with the difference in roughness of the substrate and the substantial variation in droplet volume.

On the other hand, the behaviour of the UV-curable resin matches with the wettability previously observed, where the drops are bigger on the polycarbonate film and slightly smaller on the carbon substrate. In the case of the photoactive resin on a substrate of the same material there are no droplets to observe, which is a clear indication of the coalescence of the drops and the good wetting already observed previously. It is expected that a similar test with a smaller DPI will lead to a situation where drops could be observed before merging. This situation does not hinder the printing of multi-layered samples of photo-reactive resin, as it was previously shown in Figure 12, since the outer edge of the pattern is preserved long enough to pin it in place during the curing step.

Once both the conductive and structural materials were characterised and tested together without relevant interaction between them, a proof-of-concept sample was created to show the capabilities of the high viscosity jetting approach. To do it, the structure was divided in different "structural blocks" containing a different number of layers of each material in order to compensate their different thickness, as is described in Table 3. However, since there is an LED embedded on the sample, the thickness of the component need to be compensated as well. This resulted into the functional proof-of-concept sample shown in Figure 14, where the LED is emitting a clearly visible green light while is powered by 4.5 V.

Table 3: Description of the main "structural blocks" of a proof-of-concept sample for embedded electronics. The carbon paste acts in this case as a functional material due to its conductivity and the UV-curable resin as a structural component. An LED is manually introduced after the carbon tracks are printed.

Pattern	Material	Number of layers
	Functional (carbon paste)	5
	Structural (UV-curable resin)	10,7,4,5
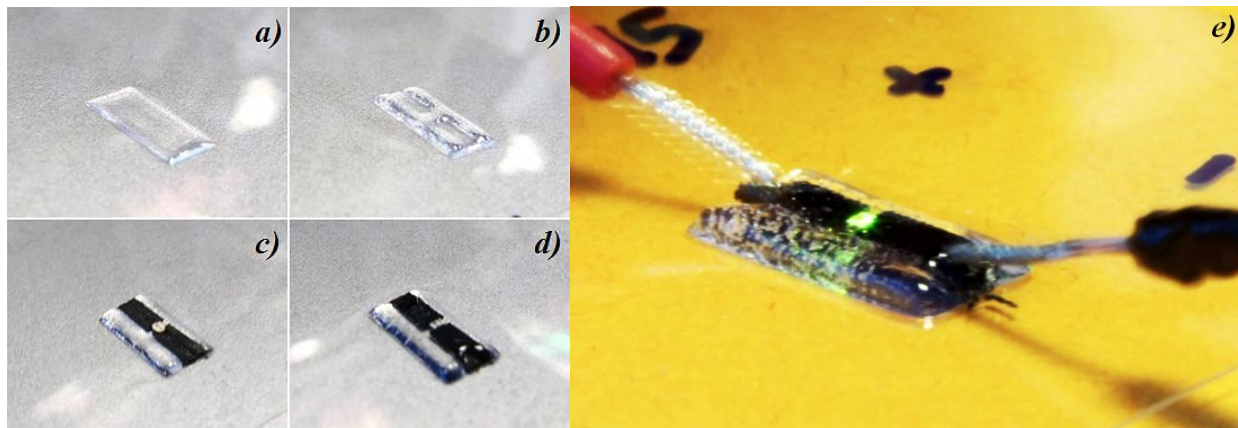
Figure 14: Embedded LED and conductive tracks proof-of-concept. a) First structural block of structural material. b) Second structural block of structural material. c) First 2 structural blocks, conductive block and LED. d) Totally embedded LED sample. e) Two probes with a voltage of 4.5 V are used to power the LED, which emits a green light.

Conclusions

This investigation studied the suitability of a high viscosity jetting valve based on the combination of pneumatic and mechanic forces as an Additive Manufacturing technique for multi-material 3-dimensional parts. Two fluids of different rheological behaviour were jetted and deposited in 2D and 3D geometries, identifying their difference in layer thickness as the main challenge for multi-material samples. This issue was minimised by the printing of "structural blocks" of equivalent height, using the values obtained during the characterization of multi-layered tracks. Additionally, the transparency and electronic conductivity of the materials investigated were applied to the creation of a proof-of-concept sample with embedded conductive tracks and an LED. Further investigation of the influence of the material properties on the final geometry and performance of the parts is required in order to achieve the full potential of this promising approach.

Acknowledgment

References

[1]   D. Espalin, J. A. Ramirez, F. Medina, and R. Wicker, "Multi-material, multi-technology FDM: exploring build process variations," *Rapid Prototyp. J.*, vol. 20, no. 3, pp. 236–244, Apr. 2014.

[2]   L. W. Ming and I. Gibson, "Possibility of colouring SLS prototypes using the ink-jet method," *Rapid Prototyp. J.*, vol. 5, no. 4, pp. 152–154, Dec. 1999.

[3]   J.-W. Choi, H.-C. Kim, and R. Wicker, "Multi-material stereolithography," *J. Mater. Process. Technol.*, vol. 211, no. 3, pp. 318–328, Mar. 2011.

[4]   H. Gothait, "Apparatus and method for three dimensional printing WO 2000052624 A1," 2000.

[5]   T. Sekitani, Y. Noguchi, U. Zschieschang, H. Klauk, and T. Someya, "Organic transistors manufactured using inkjet technology with subfemtoliter accuracy.," *Proc. Natl. Acad. Sci. U. S. A.*, vol. 105, no. 13, pp. 4976–80, Apr. 2008.

[6]   P. Calvert, D. Duggal, P. Patra, A. Agrawal, and A. Sawhney, "Conducting Polymer and Conducting Composite Strain Sensors on Textiles," *Mol. Cryst. Liq. Cryst.*, vol. 484, no. 1, p. 291/[657]–302/[668], Apr. 2008.

[7]   V. Subramanian, J. M. J. Frechet, P. C. Chang, D. C. Huang, J. B. Lee, S. E. Molesa, A. R. Murphy, D. R. Redinger, and S. K. Volkman, "Progress Toward Development of All-Printed RFID Tags: Materials, Processes, and Devices," *Proc. IEEE*, vol. 93, no. 7, pp. 1330–1338, Jul. 2005.

[8]   S. Magdassi, Ed., *The chemistry of inkjet inks*. The Hebrew University of Jerusalem, Israel: World Scientific, 2010.

[9]   M. Hedges and A. Marin, "3D Aerosol Jet® Printing-Adding Electronics Functionality to RP/RM," in *DDMC 2012 Conference*, 2012, pp. 1–5.

[10]   S. a. Elrod, B. Hadimioglu, B. T. Khuri-Yakub, E. G. Rawson, E. Richley, C. F. Quate, N. N. Mansour, and T. S. Lundgren, "Nozzleless droplet formation with focused acoustic beams," *J. Appl. Phys.*, vol. 65, no. 9, p. 3441, 1989.

[11]   D. W. Rosen, L. Margolin, and S. Vohra, "Printing High Viscosity Fluids Using Ultrasonic Droplet Generation," in *International Solid Freeform Fabrication Symposium – An Additive Manufacturing Conference*, 2008, pp. 239–253.

[12]   H. Yang, Y. He, C. Tuck, R. Wildman, and R. Hague, "High viscosity jetting system for 3D reactive inkjet printing," in *Twenty Forth Annual International Solid Freeform Fabrication Symposium – An Additive Manufacturing Conference*, 2013, pp. 505–513.

[13]   Nordson EFD, *PICO x MOD Valve Operating Manual*, 1st ed. 2013.

[14]   David R. Lide, *CRC Handbook of Chemistry and Physics*, Internet V. Boca Raton, FL: CRC Press, 2005.

[15]   Malvern Instruments Limited, "Quantifying shear thinning behavior on a rotational rheometer using the power law model," 2014.

[16]   S. J. Leigh, R. J. Bradley, C. P. Purssell, D. R. Billson, and D. a Hutchins, "A simple, low-cost conductive composite material for 3D printing of electronic sensors.," *PLoS One*, vol. 7, no. 11, Jan. 2012.